

## A SEARCH FOR WATER VAPORIZATION ON CERES\*

P. ROUSSELOT<sup>1</sup>, E. JEHIN<sup>2</sup>, J. MANFROID<sup>2</sup>, O. MOUSIS<sup>1</sup>, C. DUMAS<sup>3</sup>, B. CARRY<sup>4</sup>, U. MARBOEUF<sup>5</sup>, AND J.-M. ZUCCONI<sup>1,6</sup>

<sup>1</sup> Observatoire de Besançon, Institut UTINAM-UMR CNRS 6213, University of Franche-Comté, BP 1615, 25010 Besançon Cedex, France; roussetot@obs-besancon.fr

<sup>2</sup> Institut d'Astrophysique et de Géophysique, Université de Liège, Allée du 6 août 17, B-4000 Liège, Belgium

<sup>3</sup> European Southern Observatory, Alonso de Cordova 3107, Vitacura, Casilla 19001, Santiago 19, Chile

<sup>4</sup> European Space Astronomy Centre, ESA, P.O. Box 78, 28691 Villanueva de la Cañada, Madrid, Spain

<sup>5</sup> Institut de Planétologie et d'Astrophysique de Grenoble, Université Joseph Fourier, CNRS INSU, France

Received 2011 April 15; accepted 2011 July 18; published 2011 September 14

### ABSTRACT

There are hints that the dwarf planet (1) Ceres may contain a large amount of water ice. Some models and previous observations suggest that ice could be close enough to the surface to create a flux of water outward through the regolith. This work aims to confirm a previous detection of OH emission off the northern limb of Ceres with the *International Ultraviolet Explorer (IUE)*. Such emission would be evidence of water molecules escaping from the dwarf planet. We used the Ultraviolet and Visual Echelle Spectrograph of the Very Large Telescope to obtain spectra off the northern and southern limbs of Ceres at several epochs. These spectra cover the 307–312 nm wavelength range corresponding to the OH (0,0) emission band, which is the brightest band of this radical, well known in the cometary spectra. These new observations, five times more sensitive than those from *IUE*, did not permit detection of OH around Ceres. We derive an upper limit for the water production of about  $\sim 7 \times 10^{25}$  molecules  $s^{-1}$  and estimate the minimum thickness of the dust surface layer above the water ice layer (if present) to be about 20 m.

*Key words:* minor planets, asteroids: individual (Ceres)

*Online-only material:* color figures

### 1. INTRODUCTION

The dwarf planet (1) Ceres and the asteroid (4) Vesta are targets of the NASA *Dawn* mission (e.g., Russell et al. 2004, 2007). With a diameter of 935 km (Carry et al. 2008), Ceres is by far the largest body in the asteroid belt, and its water content could range between 0% (Zolotov 2009) and more than 20% by mass (McCord & Sotin 2005; Castillo-Rogez & McCord 2010) depending on the mineral composition considered. This water content is derived from its bulk density, estimated to be 2077 kg  $m^{-3}$  according to Thomas et al. (2005) or 2206 kg  $m^{-3}$  according to Carry et al. (2008). This object appears to be a unique remnant of the primitive asteroid belt that would have lost 99.9% of its primordial mass (Morbidelli et al. 2009) and it is now considered representative of the protoplanets that formed terrestrial planets in the early stages of the solar system.

This estimate of water content is consistent with *Hubble Space Telescope* observations which suggest that Ceres's shape is the result of a rocky core surrounded by an ice-rich mantle (Thomas et al. 2005). Observational evidence of hydration on Ceres is, however, weak. In the IR spectrum, it is particularly difficult to assess the existence of hydration on Ceres. Lebofsky et al. (1981) studied the 3  $\mu m$  region in the spectrum of Ceres and detected a strong absorption at 2.7–2.8  $\mu m$  due to structural OH groups in clay minerals. They also pointed out a narrow absorption feature at 3.1  $\mu m$  which was attributed to a very small amount of water ice. This absorption feature at 3.06  $\mu m$  was later reinterpreted by King et al. (1992) as a signature of ammoniated phyllosilicate. Vernazza et al. (2005) could reproduce the same feature with a linear mixture of crystalline ice and residue of ion-irradiated

asphaltite. A new high-quality data set led to a further reinterpretation of the 3.06  $\mu m$  band as due to an iron-rich clay (Rivkin et al. 2006) but Milliken & Rivkin (2009) modeled the same data set with brucite (see Rivkin et al. 2010 for a review). These observations are supported by the evidence of hydrated minerals in meteorites. Most of these minerals formed as a result of water ice accreting with the chondritic meteorite parent bodies, melting, and driving aqueous alteration reactions (Clayton & Mayeda 1996; Jewitt et al. 2007).

Fanale & Salvail (1989) developed an analytical model that describes the water regime of Ceres. They found that water ice could have survived 4.5 Gyr at a depth of only 10–100 m near the equator and less than 1–10 m at latitudes greater than 40°. They estimated the global water supply rate to be between 30 and 300 g  $s^{-1}$  (i.e., between  $10^{24}$  and  $10^{25}$  molecules  $s^{-1}$ ).

Long-exposure *International Ultraviolet Explorer (IUE)* spectra off the southern and northern limbs of Ceres were obtained by A'Hearn & Feldman (1992; hereafter AHF) to explore the possibility that OH resulting from the photodissociation of sublimated water vapor might escape. They reported a marginal ( $1\sigma$ ) detection of OH above the northern limb after perihelion while no evidence of this radical was found off the southern hemisphere before perihelion. This result is consistent with OH escaping from a north polar ice cap that may dissipate in summer and is replenished in winter via subsurface percolation. The inferred globally integrated production rate based on this detection was  $\simeq 1.4 \times 10^{26}$  molecules  $s^{-1}$ , i.e., superior by at least one order of magnitude to Fanale & Salvail's estimation.

This paper presents new observational data to test AHF's detection. In Section 2, the data are described. In Section 3 we present our data processing and analysis and Section 4 is a discussion about the non-detection and how it can be interpreted.

### 2. OBSERVATIONS

Ceres was observed in 2007 and 2009 at the European Southern Observatory using the 8.2 m UT2/Kueyen telescope

\* Based on observations collected at the European Organisation for Astronomical Research in the Southern Hemisphere, Chile-program ID: 080.C-0881.

<sup>6</sup> Deceased.

**Table 1**  
Observing Circumstances

UT Start	$X$	$R$	$\Delta$	$V_R$	$V$	Limb	Offset	Slit	Seeing	Sky
2007 Oct 24–04:44	1.22	2.83	1.88	−1.34	7.5	South	4.5	3	0.55	PHO
2007 Oct 24–05:37	1.20	2.83	1.88	−1.34	7.5	North	4.0	3	0.55	PHO
2007 Dec 5–03:20	1.22	2.79	1.91	−1.43	7.9	North	1.8	1	0.6	PHO
2007 Dec 21–02:00	1.22	2.78	2.03	−1.45	8.0	North	2.5	1	0.6	CLR
2009 Jan 25–06:08	1.57	2.55	1.73	−0.10	7.4	North	1.0	1	0.7	PHO
2009 Feb 23–06:29	1.57	2.55	1.58	0.08	6.9	North	1.2	1	0.5	PHO
2009 Mar 23–02:26	1.63	2.55	1.67	0.26	7.3	North	1.2	1	0.6	PHO
2009 Apr 1–01:53	1.61	2.55	1.74	0.31	7.4	North	1.1	1	0.65	PHO
2009 Apr 1–02:46	1.57	2.55	1.74	0.31	7.4	South	1.5	1	0.65	PHO

**Notes.**  $X$ : airmass;  $R$ : heliocentric distance (AU);  $\Delta$ : geocentric distance (AU);  $V_R$ : heliocentric radial velocity ( $\text{km s}^{-1}$ );  $V$ : visual magnitude of Ceres. The offset represents the distance between the center of the slit and the Ceres center of light (arcseconds), the slit being oriented perpendicular to the spin axis. This offset corresponds to the value computed during the data processing (see the end of Section 3.1). Slit: slit width (arcseconds). The seeing is expressed in arcseconds. For the sky column, PHO stands for photometric and CLR indicates clear. The exposure time was 2850 s for all exposures and the slit length was always the same ( $10''$ ).

of the Very Large Telescope (VLT) with the Ultraviolet and Visual Echelle Spectrograph (UVES; Dekker et al. 2000). This instrument is a cross-dispersed echelle spectrograph designed to operate with high efficiency from the atmospheric cutoff at 300 nm to the long wavelength limit of the CCD detectors (about 1100 nm). To this aim, the light beam from the telescope is split into two arms (UV to blue and visual to red) within the instrument. Ceres was observed with the blue arm centered at 346 nm, with a resolving power of  $\lambda/\Delta\lambda$  varying from  $\simeq 15,000$  to  $\simeq 45,000$ , depending of the width of the slit.

The slit was oriented perpendicular to Ceres’s spin axis, either above the northern limb or below the southern limb, Ceres being positioned outside the slit. The observations were performed in service mode in order to get very good seeing and place the slit as close as possible to Ceres. Two series of data were obtained, one with a wide  $3''$  slit placed about  $3''$  from Ceres’s centroid and one with a narrow  $1''$  slit at different distances from Ceres’s center of light. All exposures were obtained with an exposure time of 2850 s. The observing circumstances are summarized in Table 1.

### 3. DATA PROCESSING AND ANALYSIS

#### 3.1. Data Processing

The spectra were reduced using the spatial extraction (line by line) mode of the UVES pipeline (Ballester et al. 2000). The cosmic rays were rejected and the master response curve for each setting and extinction law were applied to get a flux calibrated spectrum. For each epoch we obtained (1) a two-dimensional spectrum with 18 lines over the  $10''$  slit length and (2) a one-dimensional spectrum corresponding to the merging of all 18 lines, excluding spatial information.

The sunlight reflected on Ceres and scattered through the nearby slit had to be removed from the spectra. Even with sub-arcsecond seeing the slit was almost tangent to the very bright image of Ceres, and there was a strong background gradient across the width of the slit.

To remove this superimposed solar spectrum, we used the BASS2000 spectrum (Paletou et al. 2009) with the appropriate Doppler shift and a convolution with a slit profile determined iteratively. At each step of the iteration, the intensity of the solar spectrum was estimated by minimizing the residual features on

the subtracted spectrum. The procedure was carried out for each one-dimensional spectrum.

Since OH radicals are also present in the terrestrial atmosphere it is possible that some weak OH emission lines are absorbed by the terrestrial OH radicals. To verify this possibility, we have searched for OH absorption lines in very high signal-to-noise (S/N) spectra of hot stars (Bagnulo et al. 2003) without success. Another important argument against such a possible contamination by OH telluric lines is the Doppler shift owing to the topocentric velocity of Ceres. This Doppler shift is about  $0.1 \text{ \AA}$ , i.e., much higher than the real width of OH lines.

The lines of the two-dimensional spectra were merged in order to obtain spectra at six positions across the slit length. The scattered background was estimated by adjusting the background already determined for the whole one-dimensional slit spectrum. All spectra were calibrated by comparison with the entire slit-calibrated spectra derived by the UVES pipeline. The results were converted in terms of radiance ( $\text{erg s}^{-1} \text{ cm}^{-2} \text{ arcsec}^{-2} \text{ \AA}^{-1}$ ).

Because of the tracking uncertainty, the distance between the center of the slit and the apparent disk of Ceres, which was small (most of the time  $< 2''$ ), varied slightly during the exposures. We therefore computed the effective distance from the scattered background. The slit was approximately parallel to the ecliptic, i.e., to Ceres’s equator, because its obliquity on its own orbit—inclined on the ecliptic by  $10^\circ 5'$ —is about  $4^\circ$  (Carry et al. 2008). Because of the slit length such an angle is negligible for a potential polar water ejection. To obtain effective distances, we modeled the scattered background for each observation. The adopted set of values reproduces reasonably well the above-determined scattered spectrum radiance at every position. The absolute position of each slit element could then be calculated and converted in projected distances in kilometers.

#### 3.2. Analysis

The main issue is the background subtraction. In order to get the best data we decided to combine the spectra obtained at different epochs in four different projected distance ranges after proper rebinning to enhance the S/N: (1) less than 2500 km, (2) 2500–5000 km, (3) 5000–7500 km, and (4) more than 7500 km. Figure 1 presents the resulting spectra (raw spectrum, solar spectrum, and the difference). There is a large decrease of noise in the final solar subtracted spectrum with increasing projected

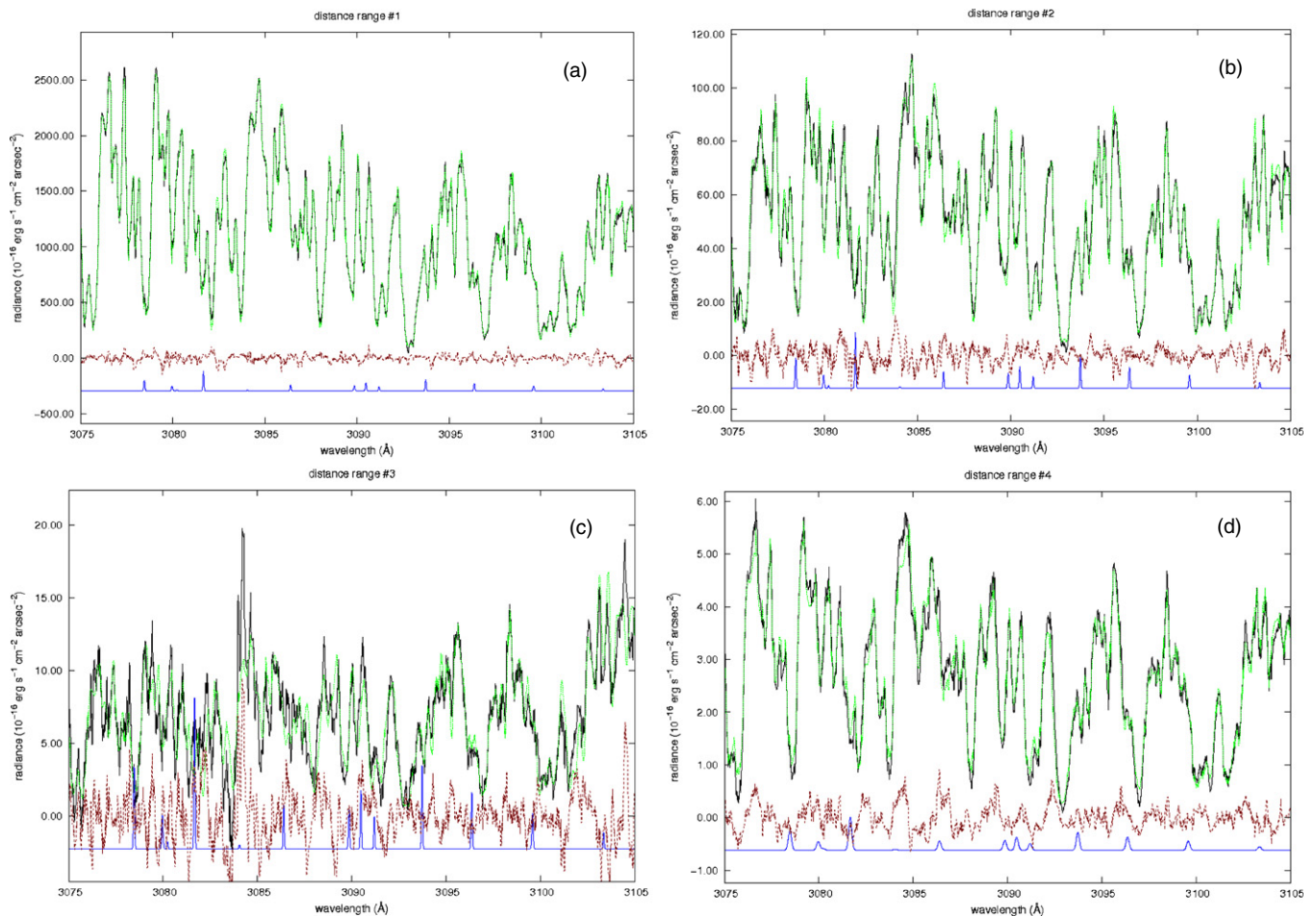


**Figure 1.** Individual spectra obtained for four different distance ranges: (a) less than 2500 km, (b) 2500–5000 km, (c) 5000–7500 km, and (d) more than 7500 km. Each figure represents the average flux-calibrated observed spectrum for the considered distance range (upper line, black), the solar spectrum adjusted to the previous spectrum (green line), the residual spectrum, i.e., average flux-calibrated spectrum minus solar spectrum (red line), and the synthetic OH spectrum adjusted in intensity to permit detection (blue line).

(A color version of this figure is available in the online journal.)

**Table 2**

Upper Limits for the Radiance of the OH (0,0) Band (Sum of the 14 Brightest Lines) for the Different Distance Ranges

Distance Range (km)	Radiance 1 ( $10^{-16}$ erg $\text{cm}^{-2}$ arcsec $^{-2}$ s $^{-1}$ )	Radiance 2 (Rayleigh)
< 2500	60	480
2500–5000	7	56
5000–7500	3.5	28
> 7500	0.6	5
Avg 2007 Oct 24	0.6	5

distance to Ceres. Simulated OH spectra for the conditions of the 2007 observations have been superimposed (blue line) at a  $2\sigma$  level which should have allowed easy detection.

We also co-added the two full-slit spectra obtained on 2007 October 24. The resulting spectrum is essentially equivalent to the average spectrum shown in Figure 1(d) because those spectra have been taken at the greatest distances from Ceres. They have the advantage of better extraction over the slit compared to the short sections. The result is shown in Figure 2.

We adopted the values of the integrated radiance of the synthetic spectra over the (0–0) band as conservative upper limits of the OH radicals (see Table 2). The spectra obtained far from Ceres on 2007 October 24 are the best for deriving an

upper limit of the OH production rate due to their much weaker sunlight contamination. The final upper limit of the radiance, taking into account all spectra, is the same as that for the data set of the spectrum shown in Figure 1(d) but corresponds to a slightly more important distance and, consequently, to a slightly more important water production rate (because the integrated number of OH molecules along the line of sight would be smaller for the same water production rate). As a consequence we used only the first two spectra and their associated upper limit for the OH radiance to derive an upper limit for the water production rate.

Figure 2 presents the results of averaging the two spectra obtained on 2007 October 24. The mean OH profile obtained by summing the flux in the expected position of the 14 brightest OH lines in the range 3070–3110 Å is also shown. No OH emission line is detected. Our final estimation of the upper limit for the integrated radiance is based on the data used for this plot. The other spectra unfortunately could not be used to improve the sensitivity of our observations. The influence of Ceres’s scattered light was far more important than expected for these spectra. This phenomenon should be taken into account in future attempts to repeat such observations with any bright source.

Using the fluorescence efficiency (“g factor”) of the 14 brightest OH lines of the (0,0) band, we derive an upper limit for the average column density of OH radicals for the slit.

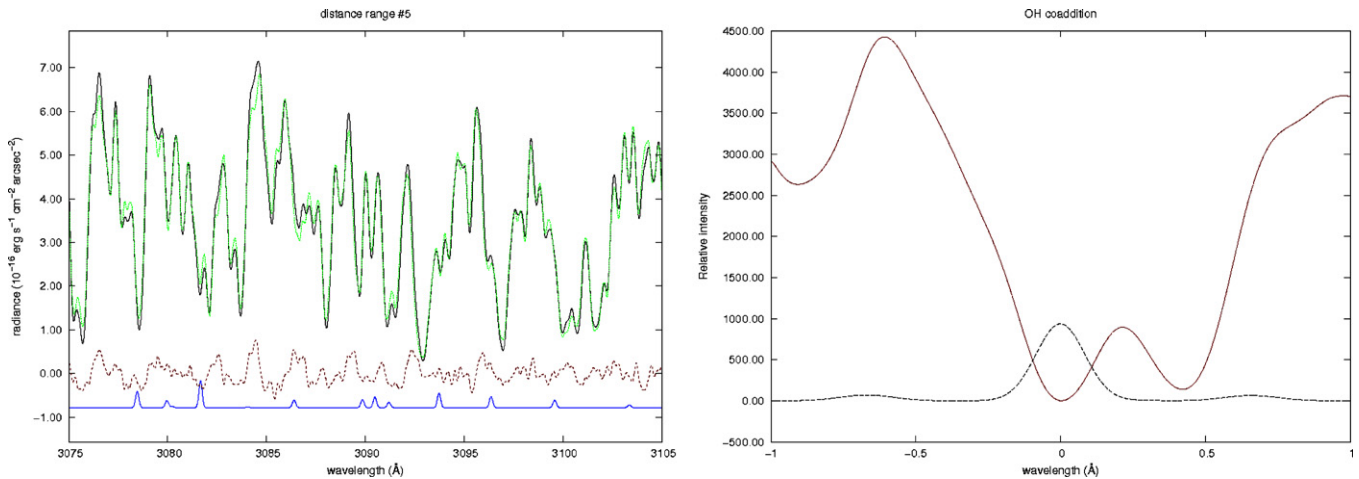


**Figure 2.** Left: average of the two first spectra from Table 1. The colors are the same as in Figure 1. Right: mean OH spectrum obtained by summing the flux of the 14 brightest OH lines in the range 3070–3110 Å and averaged for the two spectra obtained on 2007 Oct 24. The upper red line is obtained from the observational spectra and the lower black line from the theoretical spectrum. No emission line corresponding to the synthetic spectrum can be detected.

(A color version of this figure is available in the online journal.)

We used a cometary OH fluorescence model (Hutsemékers et al. 2008) to compute a value of  $2.779 \times 10^{-5}$  photon  $s^{-1}$  molecule $^{-1}$  for the considered heliocentric distance. These lines represent 86% of the total (0,0) band intensity. From Table 2 and this  $g$  factor, we can derive an average column density of  $1.80 \times 10^{11}$  molecules  $cm^{-2}$  for the slit geometry. For a better comparison with the value published by AHF—which is  $2.80 \times 10^{11}$  molecules  $cm^{-2}$ —we need to take into account the difference in observational geometry.

To compare these two values we need to compute the ratio of the average column densities for two different slits, corresponding to our observations with UVES and those of AHF with *IUE* with the same water production rate. To achieve this computation and also to estimate the corresponding upper limit for the water production rate, we have developed a Monte Carlo model based on a cometary coma model (Combi & Delsemme 1980) but adapted for a planetary body with significant gravity. The escape velocity from Ceres can be computed from its mean radius (467.6 km; Carry et al. 2008) and its mass ( $4.76 \times 10^{-10} M_{\odot}$  from the average of the results published by Kovačević & Kuzmanoski 2007). These data lead to an escape velocity of  $520 \text{ m s}^{-1}$ . Ceres’s average surface temperature, computed from its orbital elements, albedo, and the thermal conductivity of a dust layer (see the subsurface model presented in Section 4) is close to 167 K. With such a temperature about 53% of water molecules that escape from Ceres remain gravitationally bound to it (from the formulae by Fanale & Salvail 1989). If Ceres has an atmosphere it is an intermediate case between the bound atmosphere of a typical planet and the freely outflowing atmosphere of a comet.

We have tested two different possibilities for the ejection of water molecules. The first one is based on an initial ejection velocity given by a Maxwellian distribution with  $T = 167 \text{ K}$  which likely represents well the average kinetic temperature of a hypothetical atmosphere close to Ceres’s surface. Such a model provides an average ejection velocity from Ceres of  $443 \text{ m s}^{-1}$ , i.e., close enough to the escape velocity to permit a significant number of molecules to escape ( $\sim 100\text{--}53 = 47\%$  according to Fanale & Salvail 1989, as mentioned above). The second model was based on a constant radial ejection velocity computed from the formula given by Cochran & Schleicher (1993):  $v = 850 R_h^{-0.5}$  with  $R_h$  being the heliocentric distance

(AU) and  $v$  the parent velocity ( $\text{m s}^{-1}$ ). For  $R_h = 2.88 \text{ AU}$  one finds  $v = 505 \text{ m s}^{-1}$ , i.e., also very close to the escape velocity, but with no dispersion, contrary to the Maxwellian distribution.

For both models molecules move radially away from Ceres with a decreasing velocity due to the gravity field until they are photodissociated by solar radiation. During their photodissociation we consider that 91.8% of water molecules create OH radicals, with an average ejection velocity of  $1050 \text{ m s}^{-1}$  (Crovisier 1989). If OH radicals are photodissociated later than the time chosen as equilibrium time—i.e., seven times the lifetime of water molecules and OH radicals, as used by Combi & Delsemme (1980)—they are taken into account for the statistics: one OH radical is added to the radial distance located at equilibrium time. We computed the trajectory of  $10^7$  water molecules before determining statistics, which provided a few percent accuracy for the final integrated density. The lifetimes used for our model are taken from Cochran & Schleicher (1993) for water molecules (assuming a quiet Sun) and Schleicher & A’Hearn (1988) for OH radicals. Finally, OH radicals are integrated along the line of sight according to the impact parameters and integrated for the slit geometry corresponding to the observing circumstances mentioned in Table 1.

For a closer comparison with AHF’s results, we have also modified our model to use a similar hypothesis. We have assumed that water molecules stay near Ceres (at 200 km) and we have taken a constant and radial OH outflow of  $500 \text{ m s}^{-1}$ .

The results provided by the three different models are given in Table 3. This table presents both the water production rates that can be derived from UVES data (the upper limit) and from *IUE* data, as well as the extrapolated upper limit of the column density for UVES data for a similar geometry of *IUE* data.

Table 3 shows that, with a similar hypothesis (model 3), we derive a very similar water production rate for *IUE* data when compared to AHF’s results ( $1.5 \times 10^{26}$  molecules  $s^{-1}$  versus  $1.4 \times 10^{26}$  molecules  $s^{-1}$ ). We also have very similar values for the three different models of column density. The extrapolated values of upper limits from UVES data are  $\simeq 5$  times smaller than that published by AHF for *IUE* data ( $2.8 \times 10^{11}$  molecules  $cm^{-2}$ ).

From Table 3, deriving upper limits for water production rates appears more difficult. This value is more sensitive to the parameters used for modeling and varies from  $2.4 \times 10^{25}$

**Table 3**  
Total Water Production Rates (molecules  $s^{-1}$ ) Computed with Spherical Symmetrical Models

Model	1	2	3
UVES data	$7.4 \times 10^{25}$	$5.4 \times 10^{25}$	$2.4 \times 10^{25}$
<i>IUE</i> data	$3.9 \times 10^{26}$	$3.1 \times 10^{26}$	$1.5 \times 10^{26}$
Col. density	$5.9 \times 10^{10}$	$5.4 \times 10^{10}$	$5.1 \times 10^{10}$
Ratio	4.7	5.2	5.5

**Notes.** Model 1: a thermal Maxwellian distribution for water molecule velocity. Model 2: a constant velocity derived from coma cometary models. Model 3: similar to AHF's model. See the text for more details. Col. density: average column density (molecules  $cm^{-2}$ ) of UVES data when extrapolated for a similar *IUE* slit geometry. Ratio: ratio of the average column density computed by AHF for *IUE* data by the column density mentioned above. UVES data are upper limits.

to  $7.4 \times 10^{25}$  molecules  $s^{-1}$ . We believe that our first model is probably less approximate than the one presented by AHF; nevertheless, all three models are based on the assumption of spherical symmetry, which is, of course, questionable.

#### 4. DISCUSSION

The contradiction between AHF's observations and our failure to detect any OH emission with a five-times-greater sensitivity could be explained by transient  $H_2O$  emission (for instance, a plume or a cometary-like jet coming from an active region). It could also be that this first detection was spurious because the *IUE* detector's limitations, especially at the edge of the wavelength range where sensibility is low and the OH feature is observed.

Unfortunately, our limits do not permit us to test Fanale & Salvail's (1989) prediction. They proposed a production rate between 30 and 300  $g s^{-1}$  which corresponds to  $Q_{H_2O} = 10^{24}$ – $10^{25}$  molecules  $s^{-1}$ , i.e., inferior to our derived water production rate, irrespective of the model used (see Table 3).

The pole solution published by Carry et al. (2008) allows us to compute the coordinates of the sub-Earth point (SEP) and the subsolar point (SSP; see IAU recommendations from Seidelmann et al. 2007) during the observations (Table 4). Similar calculations were conducted for the previous observations by AHF. If the activity detected by AHF is due to a spot of different composition on Ceres's surface these coordinates can help to constrain this possibility. From the SSP it is also possible to see that AHF's observations were conducted at the end of northern autumn and winter while our observations were conducted at the end of northern summer. Because of Ceres's small obliquity these different seasons imply only a small change for the position of the regions heated by the Sun. This small deviation is unlikely to explain an important change in potential cometary activity. It is important to point out that, because of Ceres's rotational period (9.074 hr) and the very long exposure time of AHF's observations, Ceres was observed during an entire rotation period by *IUE*. Our own observations, conducted with shorter exposure times, correspond to more restricted areas of Ceres's surface. It is also important to point out the small difference in Ceres's heliocentric distance between the *IUE* detection (2.66 AU, after the perihelion) and the UVES observations (2.83 AU, after the aphelion). Such a small difference could hardly have a significant influence on the water sublimation rate. The probability that AHF's positive OH de-

**Table 4**  
Ceres's Heliocentric Distance ( $R$ ), SEP and SSP Coordinates (Longitude  $\lambda$  and Latitude  $\beta$ ), and Phase Angle ( $\alpha$ ) at Observing Times (Exposure Time in Minutes) for *IUE* Observations by AHF (1990 and 1991, Their Positive Detection Corresponding to 1991 Observations) and the Current Study (2007)

Date	UT (Start)	Exp. Time (m)	$R$ (AU)	$SEP_\lambda$ ( $^\circ$ )	$SEP_\beta$ ( $^\circ$ )	$SSP_\lambda$ ( $^\circ$ )	$SSP_\beta$ ( $^\circ$ )	$\alpha$ ( $^\circ$ )
1990 Jan 14	21:36	550	2.64	334	-5	345	-3	11.3
1991 May 29	12:00	450	2.66	312	-4	328	-1	16.4
2007 Oct 24	04:45	47.5	2.83	23	5	16	1	7.6
2007 Oct 24	05:38	47.5	2.83	348	5	341	1	7.6

**Notes.** We used the Eproc ephemeris generator to obtain this information based on the spin vector coordinates of Ceres from Carry et al. (2008). It should be pointed out that the rotation period (544 mn) is roughly equal to the *IUE* exposure time, i.e., these observations cover the entire Ceres rotation. For UVES observations, the longitude variation corresponds to  $\pm 15^\circ$  around these values.

tection was due to a spot on Ceres's surface seems questionable because in an observational study performed in the near-infrared (1.17–1.32 and 1.45–2.35  $\mu m$  range) Carry et al. (2011) did not find any spectral variation above 6%, which suggests a very homogeneous surface at a 50 km scale.

The upper limit for the presence of OH radicals around Ceres, as well as a close examination of the previous works published on Ceres, allows us to derive some constraints on the distribution of water in the subsurface of Ceres. We used a model of a cometary nucleus (Marboeuf 2008; Marboeuf et al. 2011) that considers an initially homogeneous sphere composed of a predefined porous mixture of ice and refractory elements (dust) in specified proportions. This model describes heat transmission, gas diffusion, sublimation/recondensation of volatiles within the nucleus, dust release, and mantle formation.

In our model, we have assumed that Ceres has an average bulk density of  $\sim 2206$   $kg m^{-3}$  (Carry et al. 2008) and a global ice content of  $\sim 10\%$  (Morbidelli et al. 2000). Assuming that the refractory part of the dwarf planet is essentially made of CM chondrite grains with densities of  $\sim 2900$   $kg m^{-3}$ , we inferred a global porosity of  $\sim 7.5\%$ . We have assumed a central temperature of the body between 90 and 150 K, i.e., the presumed temperature range of Ceres's formation (Castillo-Rogez & McCord 2010), and the surface temperature was computed from the orbital elements, its albedo, and the thermal conductivity of the dusty regolith (taken to be equal to 4.2  $W m^{-1} K^{-1}$ ; Ellsworth & Schubert 1983). The average equilibrium temperature reached by Ceres's surface at a latitude of  $60^\circ$  is 167 K, irrespective of its assumed central temperature.

Our modeling shows that the presence of water ice on Ceres's surface would increase the water production rate to several orders of magnitude above the upper limit inferred from UVES data, irrespective of its abundance. In order to maintain a water production rate below the detection limit in those conditions, we found that a top layer made only of dust and having a thickness of at least  $\sim 20$  m is needed above the subsurface of water ice and refractory material.

#### 5. CONCLUSIONS

New observations of Ceres have been conducted with one of the most sensitive instruments available for performing spectroscopy in the near-UV range. Despite a total integration time of 95 mn with VLT, leading to a sensitivity about five times better than A'Hearn & Feldman's (1992), we did not detect any OH emission lines. Thanks to a Monte Carlo model

taking into account the gravity around Ceres we estimate that in the case of an isotropic ejection, the upper limit for the water production rate is  $(2.4\text{--}7.4) \times 10^{25}$  molecules  $\text{s}^{-1}$ , i.e.,  $\sim 5$  times smaller than the production rate estimated for the northern limb by A'Hearn & Feldman, but still greater than the theoretical prediction published by Fanale & Salvail (1989) of between  $10^{24}$  and  $10^{25}$  molecules  $\text{s}^{-1}$ . Our modeling of water on Ceres's surface shows that, if water ice is present, it is probably covered by a dust layer with a thickness of about 20 m or more.

There is no clear explanation for the contradiction between our work and the detection published by A'Hearn & Feldman. This first detection could be due to either a transient phenomenon or a defect in the composition of the *IUE* detector.

Further observations could help to improve the detection limit and to reach the theoretical value predicted by Fanale & Salvail (1989). Such observations, nevertheless, should be conducted from space because ground-based observations would involve too much observing time to improve the detection limit by one order of magnitude. The Gamma Ray and Neutron Detector (see Russell et al. 2007), on board the *Dawn* spacecraft, may enable detection of atomic hydrogen, and therefore the presence of water ice beneath Ceres's surface.

This research used NASA's Astrophysics Data System and IMCCE's *Miriade VO* tool. E.J. is a Research Associate for the Belgian FRS-FNRS and J.M. is Research Director of the Belgian FRS-FNRS.

## REFERENCES

- A'Hearn, M. F., & Feldman, P. D. 1992, *Icarus*, **98**, 54
- Bagnulo, S., Jehin, E., Ledoux, C., et al. 2003, *The Messenger*, **114**, 10
- Ballester, P., Modigliani, A., Boitquin, O., et al. 2000, *The Messenger*, **101**, 31
- Carry, B., Dumas, C., Fulchignoni, M., et al. 2008, *A&A*, **478**, 235
- Carry, B., Vernazza, P., Dumas, C., et al. 2011, *Icarus*, in press
- Castillo-Rogez, J. C., & McCord, T. B. 2010, *Icarus*, **205**, 443
- Clayton, R. N., & Mayeda, T. K. 1996, *Geochim. Cosmochim. Acta*, **60**, 1999
- Cochran, A. L., & Schleicher, D. G. 1993, *Icarus*, **105**, 235
- Combi, M. R., & Delsemme, A. H. 1980, *ApJ*, **237**, 633
- Crovisier, J. 1989, *A&A*, **213**, 459
- Dekker, H., D'Odorico, S., Kaufer, A., Delabre, B., & Kotzlowski, H. 2000, *Proc. SPIE*, **4008**, 534
- Ellsworth, K., & Schubert, G. 1983, *Icarus*, **54**, 490
- Fanale, F. P., & Salvail, J. R. 1989, *Icarus*, **82**, 97
- Hutsemékers, D., Manfroid, J., Jehin, E., Zucconi, J., & Arpigny, C. 2008, *A&A*, **490**, L31
- Jewitt, D., Chizmadia, L., Grimm, R., & Prialnik, D. 2007, in *Protostars and Planets V*, ed. B. Reipurth, D. Jewitt, & K. Keil (Tucson, AZ: Univ. Arizona Press), 863
- King, T. V. V., Clark, R. N., Calvin, W. M., Sherman, D. M., & Brown, R. H. 1992, *Science*, **255**, 1551
- Kovačević, A., & Kuzmanoski, M. 2007, *Earth Moon Planets*, **100**, 117
- Lebofsky, L. A., Feierberg, M. A., Tokunaga, A. T., Larson, H. P., & Johnson, J. R. 1981, *Icarus*, **48**, 453
- Marboeuf, U. 2008, PhD thesis, Univ. de Franche-Comté
- Marboeuf, U., Mousis, O., Petit, J.-M., et al. 2011, *A&A*, **525**, A144
- McCord, T. B., & Sotin, C. 2005, *J. Geophys. Res. (Planets)*, **110**, 5009
- Milliken, R. E., & Rivkin, A. S. 2009, *Nature Geosci.*, **2**, 258
- Morbidelli, A., Bottke, W. F., Nesvorný, D., & Levison, H. F. 2009, *Icarus*, **204**, 558
- Morbidelli, A., Chambers, J., Lunine, J. I., et al. 2000, *Meteorit. Planet. Sci.*, **35**, 1309
- Paletou, F., Lafon, M., Maeght, P., et al. 2009, in *ASP Conf. Ser. 405, Solar Polarization 5: In Honor of Jan Stenflo*, ed. S. V. Berdyugina, K. N. Nagendra, & R. Ramelli (San Francisco, CA: ASP), 397
- Rivkin, A. S., Li, J., Milliken, R. E., et al. 2010, *Space Sci. Rev.*
- Rivkin, A. S., Volquardsen, E. L., & Clark, B. E. 2006, *Icarus*, **185**, 563
- Russell, C. T., Capaccioni, F., Coradini, A., et al. 2007, *Earth Moon Planets*, **101**, 65
- Russell, C. T., Coradini, A., Christensen, U., et al. 2004, *Planet. Space Sci.*, **52**, 465
- Schleicher, D. G., & A'Hearn, M. F. 1988, *ApJ*, **331**, 1058
- Seidelmann, P. K., Archinal, B. A., A'Hearn, M. F., et al. 2007, *Celest. Mech. Dyn. Astron.*, **98**, 155
- Thomas, P. C., Parker, J. W., McFadden, L. A., et al. 2005, *Nature*, **437**, 224
- Vernazza, P., Mothé-Diniz, T., Barucci, M. A., et al. 2005, *A&A*, **436**, 1113
- Zolotov, M. Y. 2009, *Icarus*, **204**, 183